



This is a repository copy of *Paper XIV (ii) A Pitting Fatigue Model for Gear Tooth Contacts*.

White Rose Research Online URL for this paper:
<http://eprints.whiterose.ac.uk/95080/>

Version: Accepted Version

Proceedings Paper:

Dwyer-Joyce, R., Hamer, J.C., Hutchinson, J.M. et al. (2 more authors) (1991) Paper XIV (ii) A Pitting Fatigue Model for Gear Tooth Contacts. In: Tribology Series. 17th Leeds-Lyon Symposium on Tribology Elsevier , pp. 391-400.

[https://doi.org/10.1016/S0167-8922\(08\)70156-1](https://doi.org/10.1016/S0167-8922(08)70156-1)

Reuse

Unless indicated otherwise, fulltext items are protected by copyright with all rights reserved. The copyright exception in section 29 of the Copyright, Designs and Patents Act 1988 allows the making of a single copy solely for the purpose of non-commercial research or private study within the limits of fair dealing. The publisher or other rights-holder may allow further reproduction and re-use of this version - refer to the White Rose Research Online record for this item. Where records identify the publisher as the copyright holder, users can verify any specific terms of use on the publisher's website.

Takedown

If you consider content in White Rose Research Online to be in breach of UK law, please notify us by emailing eprints@whiterose.ac.uk including the URL of the record and the reason for the withdrawal request.



eprints@whiterose.ac.uk
<https://eprints.whiterose.ac.uk/>

A Pitting Fatigue Life Model For Gear Tooth Contacts

R.S.Dwyer-Joyce
J.C.Hamer*
J.M.Hutchinson*
E.Ioannides†
R.S.Sayles

Tribology Section, Department Of Mechanical Engineering, Imperial College, London.

* also of PCS Ltd.

† also of SKF Engineering & Research Centre.

A model for the initiation of micro-pit fatigue failure in gear tooth contacts is presented. Micro-pitting is believed to be a surface fatigue mechanism which is highly dependent upon surface roughness and sliding conditions during the tooth contact. The model uses finite element analysis to determine local residual stresses caused by asperity flattening. These are superimposed on gear overrolling stresses and a contact fatigue life model applied. Results show that very large reductions in fatigue life can occur if asperities are plastically deformed during running-in and the contact is sliding during overrolling. Residual stress contours, fatigue life risk maps, and relative life values are given for various asperity sizes and sliding contact conditions.

1. INTRODUCTION

Micro-pitting is a major cause of gear tooth failure. The pits which are very much smaller than conventional fatigue spalls appear to initiate at, or very near to, the contacting surfaces; often causing these surfaces to take on a rather crazed appearance. The micro-pits in themselves may not be catastrophic, but failure often results either from further fatigue cracking or through excessive tooth material loss.

The formation of any fatigue pit can normally be divided into a crack initiation and crack propagation phase. The relative magnitude of these phases is often unclear but appears to be strongly influenced by the stress state, surface finish and steel cleanliness. In rolling bearings for instance, inspection of spalled raceways rarely reveals any other subsurface cracks suggesting spalling is dominated by the initiating phase. In gears though, this is not always the case and in a full treatment of micro-pitting both phases should be considered. This paper though, will only address the initiation phase of micro-pit formation.

The relatively rough surfaces found in gear teeth and the high sliding contact conditions are especially significant when considering the mechanism of gear tooth micro-pitting fatigue. In the early stages of gear operation the overrolling of the relatively rough surfaces will cause plastic flattening of the asperities. In addition the high sliding speeds may lead to the ploughing of asperities into the opposing surface. This will cause considerable plastic flow and on unloading leave subsurface residual stresses. Although in relation to the maximum contact stress these stresses may not

be particularly high, their addition to the overrolling stress distribution may have a strong influence on the pitting fatigue life.

It is essential, therefore, that any realistic fatigue life model should include the residual stress effects of asperity overrolling, indenting, and ploughing. The plastic flow can be conveniently divided into two phases; the crushing of the asperity under an applied normal and tractive force in the inlet to the ehl contact and the subsequent ploughing of the asperity into the opposing surface during its passage through the rolling/sliding contact. In this model a finite element technique is used to determine residual stresses under these types of asperity interactions. A numerical contact model is used to calculate overrolling contact pressures and from these the subsurface elastic stresses. The input to the fatigue life model is formulated from a superposition of these overrolling stresses and the residual stresses.

2. AN OVER VIEW OF THE LIFE MODEL

The determination of the fatigue life of a gear tooth contact can be divided into four basic stages.

- (i) The asperity flattening and ploughing with both friction and sliding is modelled using an elastic/plastic finite element method. From this analysis a residual stress field and an unloaded surface profile are obtained.
- (ii) The contact pressures resulting from the overrolling of the rough surface by the opposing gear tooth are derived from an elastic numerical contact model.

- (iii) These contact pressures are then used to determine the subsurface elastic stresses which are then superimposed on the residual stresses from the asperity flattening analysis.
- (iv) A discretised contact fatigue model which incorporates both a hydrostatic pressure and a limiting shear stress component in the fatigue criterion is then used to determine the fatigue life.

3. RESIDUAL STRESS DETERMINATION

3.1 Finite Element And Pre-Processing Software

The process of asperity flattening and ploughing has been modelled using ABAQUS, a general purpose finite element code. ABAQUS was developed by Hibbitt, Karlsson, and Sorensen Inc. in 1978 with a particular emphasis on non-linear analysis. Facilities are available to model accurately, gross material plasticity, large deformations, and frictional contact. These features make the program particularly suitable for this type of plastic contact analysis.

The mesh geometry was developed using SUPERTAB (part of the IDEAS suite of CAD codes developed by SDRC), as a pre-processor. A 'free' mesh generation was used which creates a somewhat irregular pattern (see Figures 1 and 2); however, the elements are all reasonably square and are much finer in the contacting region of interest. Both packages are installed on a VAX 8600 under the VMS operating system.

Three models were developed to study the asperity interaction in a gear tooth contact.

3.2 Asperity Flattening With Friction And Sliding

The first model was developed to show the elastic/plastic interaction of an asperity and opposing surface under conditions of varying friction and sliding. The model consists on two anvils, the lower with an asperity on its upper surface. The two bodies are meshed using eight noded reduced integration quadratic plane strain elements. The contact conditions are defined using six noded 'interface' elements. Figure 1 shows a diagram of mesh. The upper body is displaced onto the lower with friction and lateral movement until the asperity is fully squashed. The upper body is then moved away from the lower and the residual stress information retained. The analysis was repeated for asperity slopes of 5° and 10° with various sliding distances and friction coefficients.

3.3 Asperity Ploughing

The second model is aimed at modelling the mechanism of an asperity 'ploughing' into an opposing surface. This process is highly non-linear and requires some considerable computing power; as a result steps were taken to reduce complexity. The asperity is modelled as a rigid surface connected to the lower body by 'rigid surface interface' elements. The lower body is again made up of eight noded plane strain elements. The rigid asperity is displaced into the lower body and moved horizontally and removed. Figure 2 is a drawing of the mesh and the rigid surface asperity. Asperity slopes of 2.5° and 5° were considered and, to reduce computing time, friction was neglected.

3.4 Asperity Indentation Slope Effect

In order to study the effect of asperity slope on the residual stress field a third model was developed. To reduce computing time the analysis consisted of indenting an elastic/plastic body with a rigid asperity without friction or sliding. The lower body was again made up of a coarse mesh of eight noded plane strain elements. The rigid surface asperity was connected via 'rigid surface interface' elements. Asperity slopes of 1°, 2.5°, 5°, 7.5°, and 10° were indented and then unloaded.

4. NUMERICAL CONTACT MODEL

The final unloaded surface profile from the finite element model was retained for input to a numerical elastic contact model. In this the real surface profile is brought into contact with a smooth surface of radius of curvature equivalent to that between the mating gear teeth (1). The surface can then be divided into a series of small discrete pressure blocks, typically of 2 micron width. By simultaneous solution of the contact pressures and displacements, the approach of the two surface can be adjusted until the integrated contact pressure is equal to the tooth loading and thus the appropriate contact pressure distribution determined.

5. ELASTIC SUBSURFACE CONTACT STRESS

The subsurface is divided into a grid of square elements of the same side length as the surface pressure elements. The subsurface normal and shear stresses resulting from a surface pressure element of unit width can be expressed analytically (2). Therefore an array of influence coefficients can be developed by which the subsurface stress state at any grid point can be derived from the surface contact pressure elements. By superposition, the full subsurface stress distribution can be computed. The elastic

subsurface stress distribution at each roller location may then be obtained directly from the surface contact pressure profiles.

6. FATIGUE LIFE DETERMINATION

This technique used for fatigue life formulation was first developed by Ioannides and Harris (3). The basis for the model is a generalisation of the Lundberg-Palmgren method. Recent fatigue life tests indicate that as with most cyclic stress operations with steel components, a stress threshold exists below which the fatigue life is infinite. Furthermore rotating, bending tests have shown that the fatigue life of a component is also influenced by the prevailing hydrostatic pressures (4). Therefore the fatigue life criterion includes the full subsurface shear stress history, a hydrostatic pressure component, and a threshold shear stress. This discretised life criterion then allows for the presence of local stress effects and residual compressive or tensile hydrostatic stresses. The probability of failure is calculated from the cumulative contribution of these stresses to the fatigue criterion from small volume elements of the material.

In order to evaluate the fatigue criterion the stress state is calculated in each element for a series of positions during the overrolling of the asperity. The first part of the criterion is to determine the maximum value of $\tau_{a\theta}$ for each element. The angle at which the maximum value occurs is initially unknown so each element is tested at every overrolling position for a series of angles theta.

$$p_H = - \left[\frac{\sigma_{xx} + \sigma_{yy} + \sigma_{zz}}{3} \right]$$

$$\tau_a = \tau_{a\theta} - 0.3p_H$$

In addition the maximum absolute value of the shear stress, τ_{\max} at the critical angle in each element is found; this is used to find a shear stress limit, τ_u . This can be expressed as follows:

$$\tau_u = \tau_{\max} + 0.3p_H$$

$$\tau_u = 0.266 \text{ GPa} \quad \text{if} \quad |\tau_u| \leq 0.6 \text{ GPa}$$

$$\tau_u = 0.266 \left(1 - \frac{|\tau_u| - 0.6}{0.9 - 0.6} \right) \text{ GPa}$$

$$\text{if} \quad 0.6 < |\tau_u| \leq 0.9 \text{ GPa}$$

$$\tau_u = 0 \quad |\tau_u| > 0.9 \text{ GPa}$$

The shear stress amplitude is independent of residual or local stress effects (since it involves only the change in shear stress as the overrolling occurs). However the hydrostatic pressure and stress threshold determined from the maximum absolute value of the shear stress will be influenced by the residual stresses. A more compressive hydrostatic stress will tend to increase the stress criterion threshold. The fatigue life is then found from the volumetric integral of the fatigue life criterion.

$$\frac{1}{L^3} \sum (\tau_a - \tau_u)^{\frac{21}{5}} \delta V$$

7. RESULTS AND DISCUSSION

7.1 Finite Element Residual Stresses

The output relevant to fatigue life study, from this phase of the work, primarily consists of the residual stresses and displaced shape of the asperity surface after unloading. There exists a variety of ways of displaying this information; in this paper contours of directional stress are presented and the results discussed.

7.1.1 Asperity Flattening Residual Stresses

Figures 3 (a), (b), and (c) show XX, YY, and XY directional stress contours, for a simple flattening case with no friction and no sliding motion. The first of these plots shows that the residual X-directional stresses are largely compressive with some high tensile stresses at the asperity shoulders. As the asperity is brought into contact with the opposing surface a large compressive field is created under the contact causing radial tensile stresses to build up around the non-contacting shoulders. As the load is increased some plastic flow results within the compressive zone so that on unloading the tensile stresses can not be completely relieved. The plots of Y-directional stress again show largely compressive stresses with some low tensile stresses around the asperity axis. The third figure shows the shear stress (XY-directional) field; as might be expected the right hand side consists of positive shear (to the right) whilst the left side consists of negative shear (to the left). This is caused by the sliding motion pushing material to the side away from the axis of symmetry.

Figures 4 (a) and (b) show the effect of including friction and sliding (all sliding occurs from left to right) in the flattening process. The regions of positive shear have moved further to the right, and the line of zero shear has been displaced. This can be visualised by considering the effect of friction and sliding inducing material to be displaced to the

right. The introduction of sliding has little effect on the absolute values of all the directional stresses.

7.1.2 Asperity Ploughing Residual Stresses

Figure 5 (a), (b), and (c) show the XX, YY, and XY residual directional stresses following the rigid asperity ploughing. As before, most of the residual stresses are compressive with some tensile stresses at the dent sides. Some fairly high tensile stresses have been generated at the end (right hand side) of the ploughed furrow; caused by the building up of material at the shoulder.

Figure 6 compares the surface profiles of a ploughed furrow caused by 5° and 2.5° asperities. The smaller asperity has caused little plastic flow as the majority of the indentation can be accommodated elastically. Shoulders have been built up at both sides of the dent.

7.1.3. Asperity Slope Residual Stresses

The asperity slope indentation tests show that slope has a significant effect on the residual stress level. Although the shape of stress field contours are fairly similar the absolute values of the stresses are very dependent on asperity slope. Figure 7 shows a plot of the maximum directional stresses against asperity slope. The graph shows that for slopes of 1° and 2.5° the deformation has been largely elastic so the residual stresses are small. The magnitude of residual stress then increases rapidly with asperity slope to values in some cases of the same order as the material yield stress. These high tensile stresses generally occurred at the shoulders of the indentation.

7.2 Fatigue Life

The objective of this work is to determine the reduction in life expectancy of a surface containing real asperities over an idealised flat surface. Therefore the volume of surface under analysis has to be sufficiently large such that, at its borders the magnitude of the fatigue life criterion does not differ significantly from the smooth surface solution. Also the size of elements and number of overrolling solutions have to be optimised so that further refinement will not significantly improve the accuracy of the solution. As computing time rises rapidly with increasing refinement, some compromise must be reached, but the following dimension were found to produce summation errors of under 5%.

Asperity Size	FE Mesh	Life Mesh
width 20µm	250 x 150µm	100 x 100µm
slopes 1°, 2.5°, 5°, 10°	400 elements	2500 elements

Table 1 Grid Dimensions

The results from the fatigue life formulation have been presented in two ways. Firstly using fatigue life 'risk' maps; and secondly as a life value, relative to an undamaged flat surface.

7.3.1 Fatigue Life Risk Maps

The risk map is a contour plot of the life criterion term for each volume element. The elemental failure probability term involves raising the stress criterion to a very high power (31/3) so consequently the risk contours encompass several decades in magnitude. Therefore these have been plotted as logs to base 10.

Figure 8 shows a risk map for the flat surface case. As expected for a smooth Hertz contact the maximum amplitude of shear stress is found at the orthogonal shear stress at a distance 0.48a below the surface. With the modified criterion the effect of the hydrostatic pressure component on the threshold stress level is to push the depth of the maximum risk value a little lower to 0.52a. The wavy effect results from the discrete overrolling solutions; reducing the spacing between the solutions would reduce the wave amplitude and increase its frequency.

Figures 9 (a), (b) and (c) compare the life of an asperity with an initial slope of 5° under a purely rolling motion with the same asperity under a sliding contact with two friction coefficients of 0.05 and 0.1. These values represent approximations to two different lubrication conditions; full ehl and mixed lubrication. The effect of surface traction on life is quite dramatic; in the full ehl condition the local life reduction factor is only 2400, but increasing the friction coefficient to 0.1 causes a reduction in life of 27,000 times. The maximum elemental risk in this zone is over 10⁷ times greater than in that arising from the maximum orthogonal shear stress. Inspection of the output data indicates this life reduction is mainly caused by a drop in the fatigue threshold through an increase in the maximum absolute value of shear stress. The shear stress amplitude and hydrostatic pressure components of the fatigue criterion appear rather less sensitive to surface traction. As the bulk of this increased risk occurs in a small zone below the asperity, Figures 10 (a), (b), (c) and (d) which compare the effect of

asperity slope on life concentrate on a small 40 micron square zone under the asperity. With the 1.25° asperity, the magnitude of the near surface contours are of the same order as in the maximum orthogonal shear stress zone (Figure 8) and the life is not significantly reduced. If the asperity slope is increased to 2.5° however, a small zone builds up under the leading edge of the asperity where the life is dramatically reduced. This effect is further accentuated with the 5° slope asperity but surprisingly the life for an asperity of 10° slope does not appear to be significantly reduced. This appears to be because in both cases significant plastic flow occurs, so that the contact pressure during subsequent overrolling is approximately the same.

The net effect of the residual stresses in the rolling sliding cases is to marginally increase the overall life integral. The contribution of the tensile residual stresses appears to be largely masked by the large bulk of compressive residual stresses. Also the most significant tensile residual stresses appear to be located around the shoulders of the squashed asperity where the overrolling stresses are relatively small. In the case of a 20 micron long asperity the largest overrolling shear stresses are located in a zone approximately 3 to 8 microns ahead of the centre line and at a distance 2 to 8 microns below the surface.

The risk maps for the asperity ploughing model are shown in Figures 11 (a) and (b). Although the value of the life integral is increased over the smooth surface case it is still significantly less than that for the sliding asperity. Again the dominant effect on life arises from the high shear stresses generated under the shoulders of the dent during overrolling. However, even though some material build up occurs around the shoulders of the indentation particularly on the exit side, the contact stresses are still significantly lower than those found during the subsequent overrolling of plastically deformed asperities. The inclusion of the residual stresses (Figure 11 (b)) which are largely compressive cause an overall marked increase in the life. Although some tensile residual stresses exist around the shoulder on the exit side, they do not appear to combine dangerously with the high overrolling shear stresses.

7.3.2 Relative Fatigue Lives

As the absolute values of the life integrals under each asperity are rather difficult to interpret, they can be conveniently normalised by dividing by the value of the life integral for the equivalent volume under a flat surface. The values shown in Table 2 then indicate the factor by which the life expectancy under each asperity is reduced.

Asperity Condition	Friction Coefficient	Residual Stresses	Life Reduction Factor
Flat	0	n/a	1
Flat	0.1	n/a	1.1
5° Slope	0	N	23
5° Slope	0	Y	19
5° Slope	0.05	Y	2400
5° Slope	0.1	N	32000
5° Slope	0.1	Y	27000
2.5° Slope	0.1	N	7700
1° Slope	0.1	N	1.6
10° Slope	0	Y	20
10° Slope	0.1	Y	28000
5° Plough	0.1	N	3200
5° Plough	0.1	Y	150

Table 2 Life reduction factors under each asperity

8. CONCLUSION

In this work an elemental contact fatigue model has been used to determine the likelihood of micro-pitting arising from individual asperities contacts in a rolling/sliding gear contact. The problem has been investigated in terms of asperity slope, rolling and sliding conditions, the squashing of asperities on one surface and the consequent plastic indentation and ploughing effect on the counter surface. An FE model has been used to determine the resulting surface profile and subsurface residual stress distribution after the first initial overrolling of the virgin asperities.

The life reduction appears to be particularly sensitive to the slope of the undeformed asperity and to the presence of sliding. Asperities with slopes under about 1.5° do not appear to be at risk of micro-pitting. However the risk rises rapidly as the slope is increased up to 5°, but then levels off as the majority of the deformation becomes plastic and the contact stresses reach a limiting value. Although the size and extent of the residual stress distribution continues to increase, the more damaging tensile stresses tend to be located in sites where the overrolling stresses are relatively benign, so the two do not combine dangerously. The fatigue life appears very sensitive to surface traction. Under a pure rolling condition the life expectancy is only reduced by a factor of 19 even under a plastically deformed asperity. However in a sliding contact with a friction coefficient of 0.1

the life can be reduced by a factor of about 27,000. This reinforces the experimental evidence that micro-pitting is more prevalent with poorer finished surfaces or when the λ (film thickness/surface roughness) ratio is small. Although the effect of an asperity ploughing through the counterface causes some reduction in life expectancy this appears to be relatively small when compared to the life reduction found under the plastically deformed asperity itself.

This work represents the findings from the first stage of an investigation into gear tooth fatigue life prediction. At present the model is in a fundamental stage and only considers the interaction of individual asperities in dry contact. This is probably too severe a condition as the ehl film and subsequent material shakedown under the plastically deformed asperity will tend to reduce the magnitude of the overrolling stresses. It is planned to develop the model so that the real lubricated contact of gear teeth through the running in and steady operational phase can be simulated and thus allow a more accurate prediction of fatigue life.

REFERENCES

- [1] Webster, M. N., Ioannides, E. and Sayles, R. S. "The effects of topographical defects on the contact stress and fatigue life in rolling element bearings", Proc. of the 12th Leeds-Lyon Symposium on Tribology, Lyon, Butterworths, Vol. 12, pp. 121-131, 1985.
- [2] Johnson, K. L. "Contact Mechanics", Cambridge University Press, 1985.
- [3] Ioannides, E. and Harris, T. A. "A new fatigue life model for rolling bearings", ASME Journal Of Lubrication Technology, Vol. 107, pp. 367-378, 1985.
- [4] Dang Van, K., Griveau, B. and Message, O., (1985), "Bi-axial and multi-axial fatigue", Proc. 2nd Intl. Conf. on Multiaxial Fatigue. Mech. Eng. Publ., Sheffield, 1988.

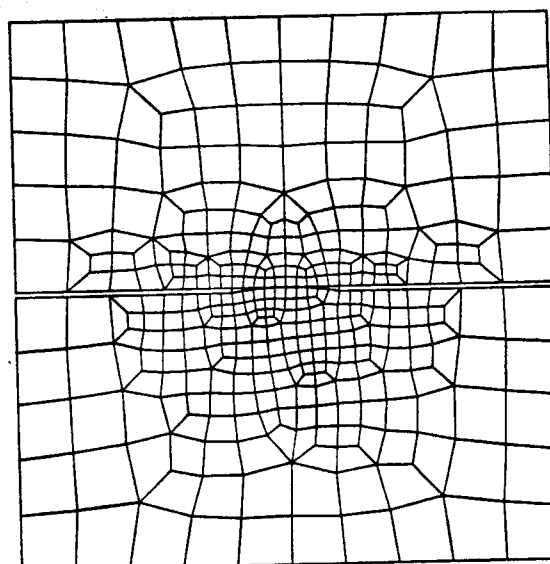


Fig. 1 Finite element mesh for asperity flattening analyses

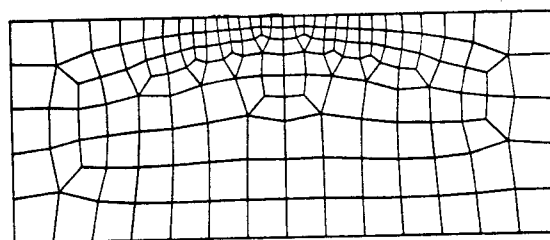


Fig. 2 Finite element mesh for asperity ploughing analyses

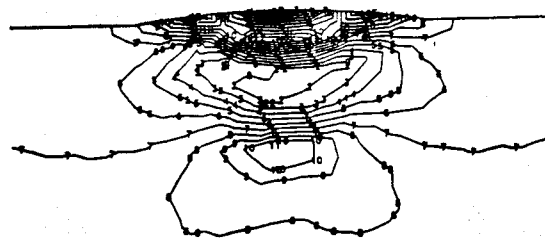


Fig. 3a Residual X-directional stresses following 5° asperity flattening (no friction)

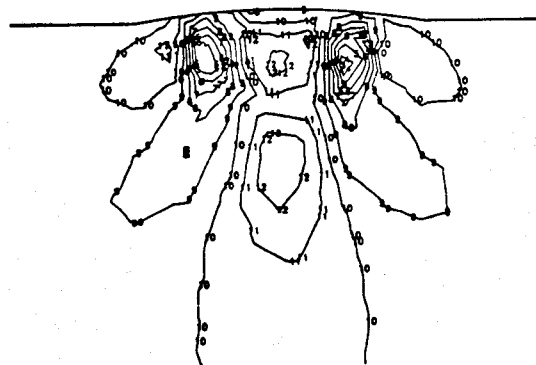


Fig. 3b Residual Y-directional stresses following 5° asperity flattening (no friction)

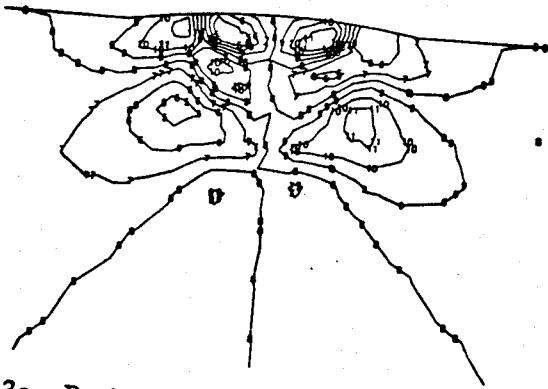


Fig. 3c Residual XY-directional stresses following 5° asperity flattening (no friction)

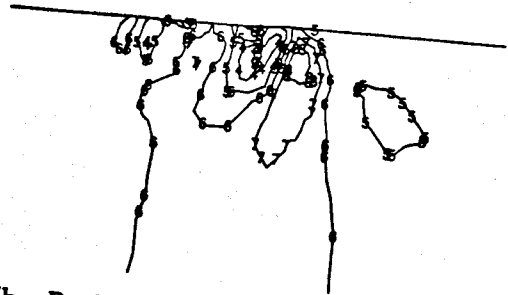


Fig. 5b Residual Y-directional stresses following 5° asperity ploughing (no friction)

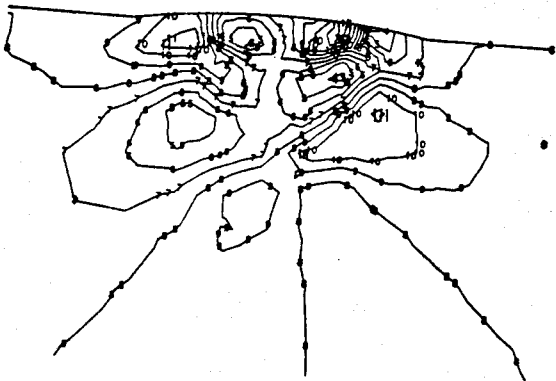


Fig. 4a Residual XY-directional stresses following 5° asperity flattening with sliding, ($\mu=0.1$)

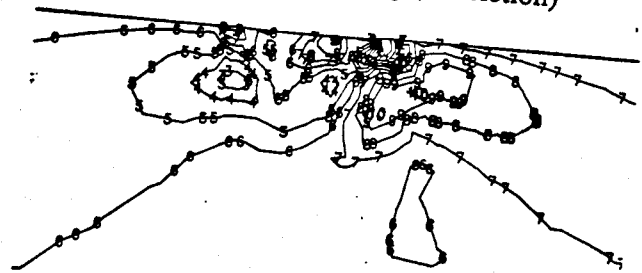


Fig. 5c Residual XY-directional stresses following 5° asperity ploughing (no friction)

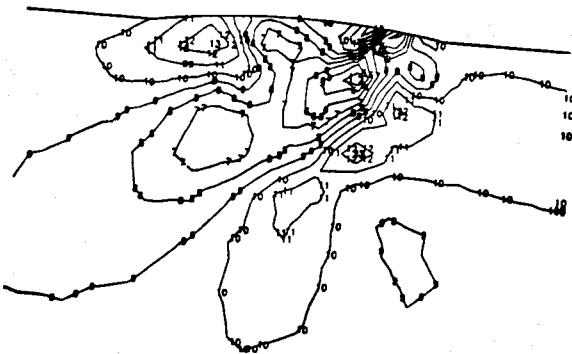


Fig. 4b Residual XY-directional stresses following 5° asperity flattening with sliding, ($\mu=0.2$)

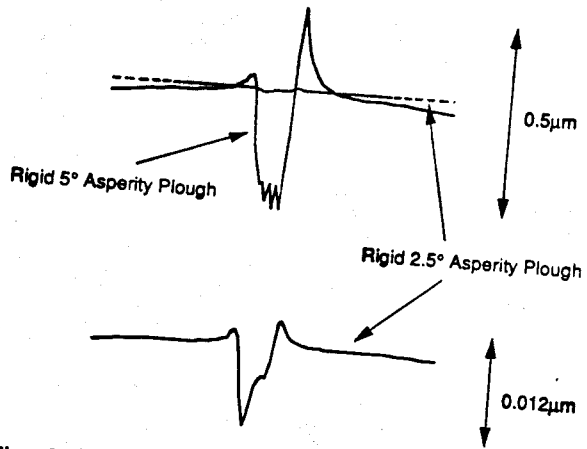


Fig. 6 Comparison of furrows caused by 2.5° and 5° rigid asperity ploughing analysis

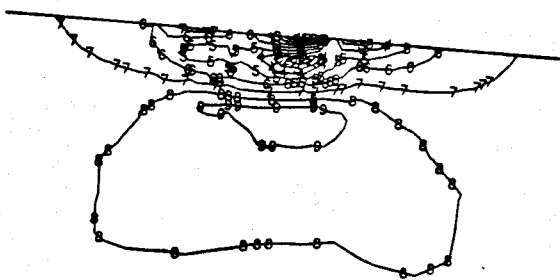


Fig. 5a Residual X-directional stresses following 5° asperity ploughing (no friction)

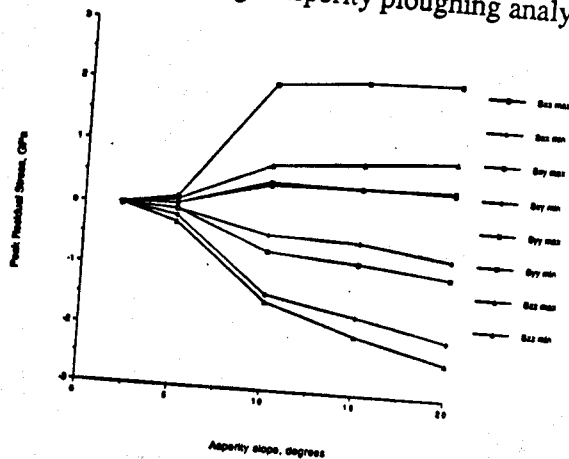


Fig. 7 Graph of asperity slope against peak residual stresses after asperity flattening

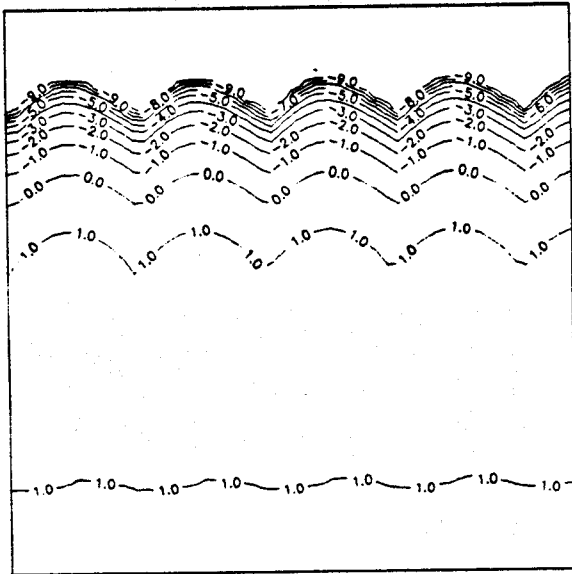


Fig. 8 100 μ m square, subsurface fatigue life risk map for a smooth surface

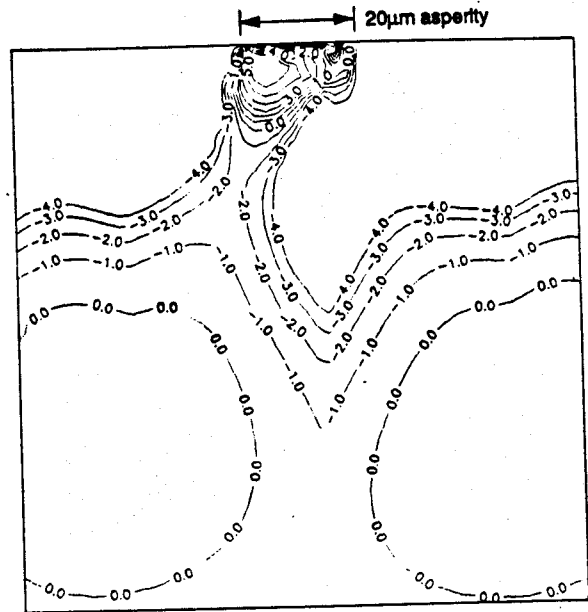


Fig. 9b 100 μ m square, subsurface fatigue life risk map for a 5° asperity overrolled with sliding, $\mu=0.05$

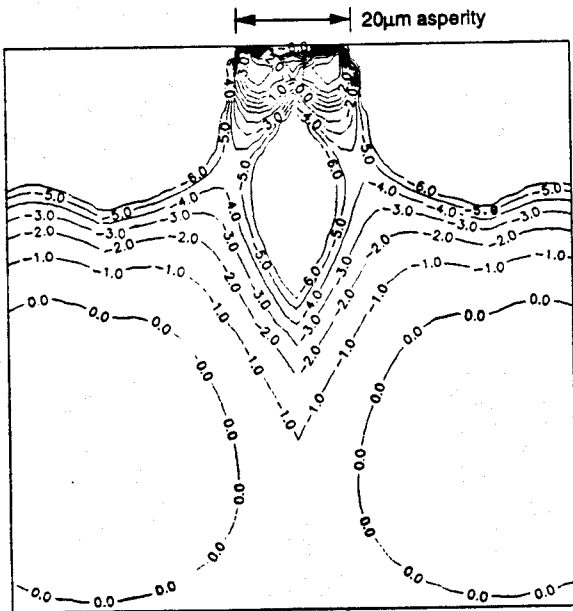


Fig. 9a 100 μ m square, subsurface fatigue life risk map for a 5° asperity overrolled without sliding

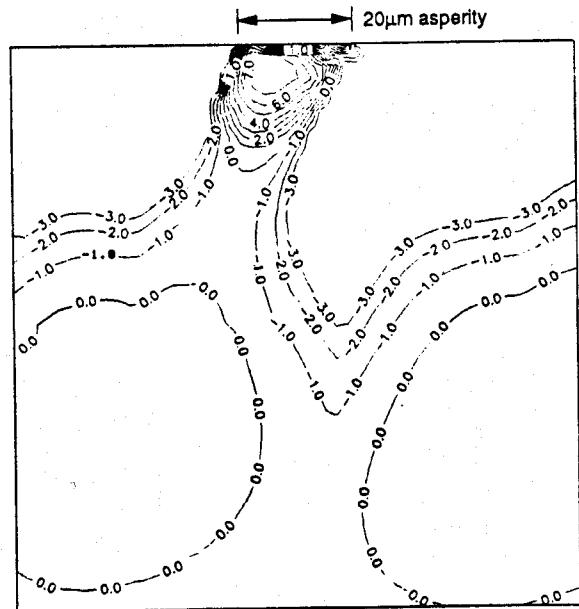


Fig. 9c 100 μ m square, subsurface fatigue life risk map for a 5° asperity overrolled with sliding, $\mu=0.1$

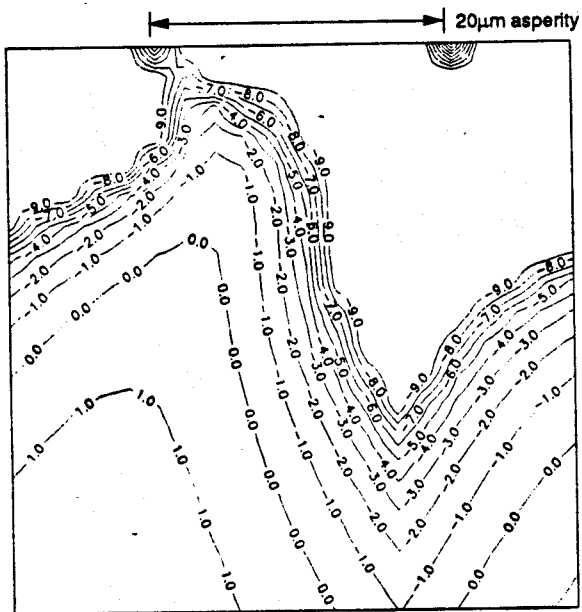


Fig. 10a 40μm square, subsurface fatigue life risk map for a 1° asperity overrolled with sliding, $\mu=0.1$

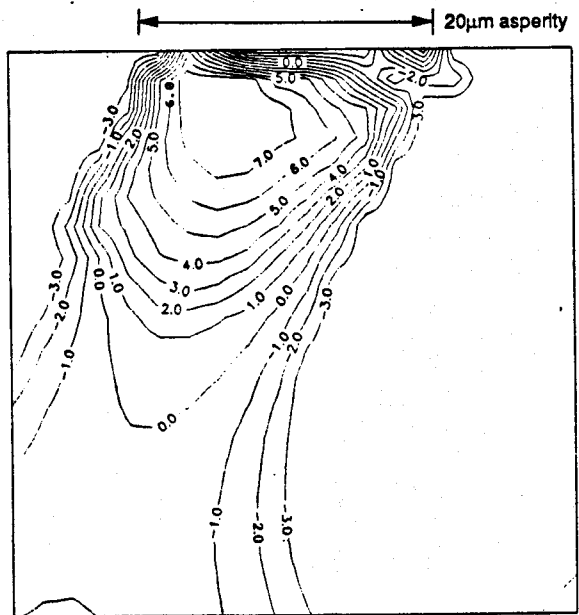


Fig. 10c 40μm square, subsurface fatigue life risk map for a 5° asperity overrolled with sliding, $\mu=0.1$

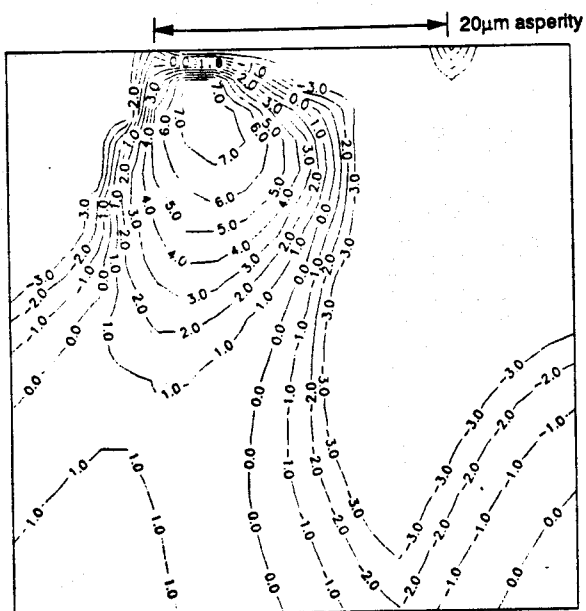


Fig. 10b 40μm square, subsurface fatigue life risk map for a 2.5° asperity overrolled with sliding, $\mu=0.1$

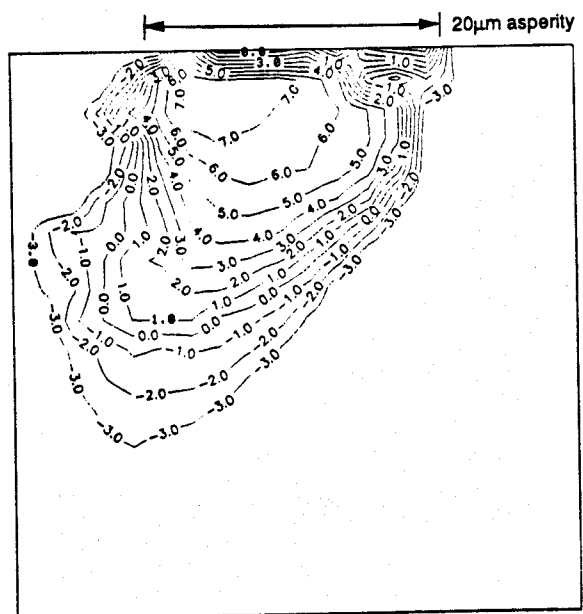


Fig. 10d 40μm square, subsurface fatigue life risk map for a 10° asperity overrolled with sliding, $\mu=0.1$

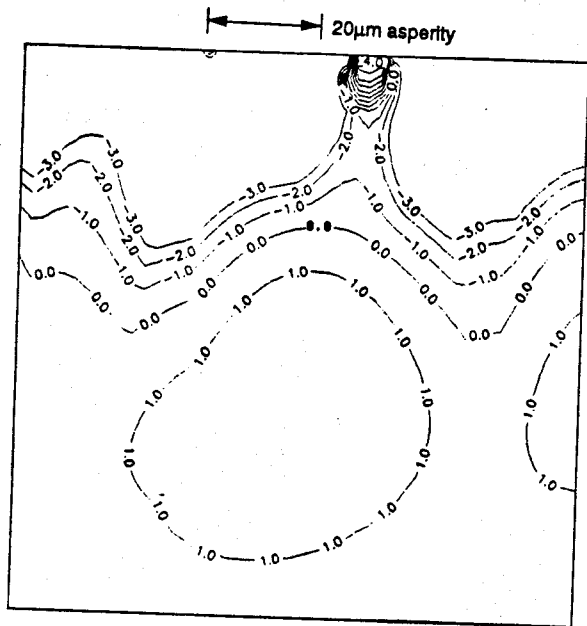


Fig. 11a 100 μ m square, subsurface fatigue life risk map for a 5 $^\circ$ rigid asperity ploughed furrow, $\mu=0.1$, without residual stresses

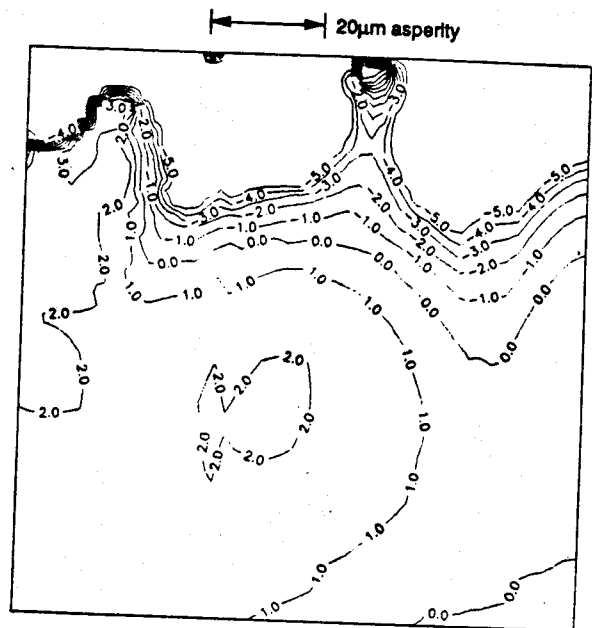


Fig. 11b 100 μ m square, subsurface fatigue life risk map for a 5 $^\circ$ rigid asperity ploughed furrow, $\mu=0.1$, with residual stresses